Centrifuge modelling of the quasi-static and dynamic behaviours of a rigid structure resting on a rigid inclusion reinforced soft ground

C. Nohra, C. Soriano-Camelo, S. Escoffier, Z. Li, L. Thorel
Univ Gustave Eiffel, GERS-CG, F-44344 Bouguenais, France
charbel.nohra@univ-eiffel.fr

ABSTRACT: The performance of a rigid inclusion (RI) foundation system was evaluated through quasi-static pushover and dynamic centrifuge tests. The analysed system considered a slender rigid structure resting on soft clay. The aim of the quasi-static pushover test was to explore the rocking response of the structure under large rotation angles, and the dynamic test examined the rocking-dominated behaviour of the structure under seismic and sinusoidal loading scenarios. The experiments were conducted at 50g using the geotechnical centrifuge at Gustave Eiffel University. The ground mass was constituted of three layers: a base layer of stiff sand, serving as the bearing substratum for the RI's; an intermediate soft clay layer in which the RI's were installed; and a surface sand layer acting as a load transfer platform (LTP). Seven aluminium tubular RI's were driven through the clay to reach the base sand layer. A stiff, cylindrical structure was positioned on top of the LTP, simulating a slender superstructure. In the quasi-static pushover test, a mechanical actuator applied a horizontal force at the centre of gravity to generate overturning moments and shear forces at the foundation level, as well as bending moments and axial loads in the RI's. In the dynamic test, the model was subjected to a sequence of base excitations. The system performance in both scenarios was assessed in terms of mobilized overturning moments, structure rotations, settlements, and internal forces in the RI's. During quasi-static pushover test, the system exhibits a markedly non-linear response, characterized by rotational stiffness degradation with increasing rotation and a cyclic overstrength associated with soil rounding and foundation uplift. Under dynamic loading, the response generally follows the monotonic pushover trend, with peak overturning moments remaining significantly lower than those obtained from quasi-static pushover tests.

1 INTRODUCTION

Soil reinforcement by rigid inclusions (RI's) is a ground-improvement technique used to enhance foundation performance by increasing bearing capacity, reducing settlements, and improving seismic stability. Although their installation resembles that of conventional pile-raft systems, RI's differ by the absence of a structural connection between the piles and the superstructure. The load transmission between the building and the RI occurs through a granular load transfer platform (LTP), which mobilizes soil arching and reduces the load carried by the inclusions. This technique, that creates a "composite foundation" has been implemented in major projects, including the Rion-Antirion Bridge, for which three of the four 90 m diameter piers are founded on 150-200 steel tubes of 2 m diameter and 25 m length, with a LTP of 2.8 m thickness (Pecker, 2004, 2006, 2023).

The seismic performance of RI's has been studied through centrifuge tests, shaking-table experiments, in-situ observations, and numerical modelling (Satheeshkumar et al., 2025). While often grouped under "unconnected piles", there is no consensus on stiffness thresholds defining RI behaviour; here, RI's refer to systems incorporating a LTP. Previous studies have examined their role in rocking foundations, showing that RI's can reduce residual settlement, modify rocking response, and enhance energy dissipation under strong shaking (Loli et al., 2015; Ha et al., 2019). However, most experimental work focuses on sand, with much less attention to clay deposits. The few studies with clay reports reduced bending moments and lateral displacements when using RI's with LTPs compared to pile-rafts and highlight the influence of LTP thickness and grain size on fuse effect (Liang et al., 2021; Yang et al., 2022,2023).

Given the scarcity of experimental data on RI's systems in clay under cyclic and seismic loadings, this study focuses on quasi-static pushover and dynamic centrifuge tests conducted on a similar configuration constituted of a soft clay layer reinforced by end bearing RI's and supporting a rigid slender structure. The advantage of quasi-static pushover tests over dynamic tests is that they permit the full mobilization of the foundation resistance through imposing the ULS loads and moments on the foundation (for a fixed vertical load, the weight of the structure in this case). The dynamic tests were conducted for the purpose of investigating the impact of RI's on Soil-Structure Interaction (SSI) and to evaluate how much of the foundation resistance is mobilized under seismic loading at different load amplitudes. The dynamic test involved a series of mono- and multi- frequency motions with different amplitudes. Figure 1 shows a cross section of the quasi-static pushover (Figure 1a) and dynamic (Figure 1b) tests and a plan view of the reinforced ground (Figure 2) (Dimensions in mm at model scale).

2 EXPERIMENTAL PROTOCOL

The tests were performed at a centrifugal acceleration of 50g, with the model scaled in accordance with established centrifuge scaling laws (Table 1, Garnier, 2007). Static scaling laws were applied for the pushover tests, while dynamic scaling laws were adopted for the dynamic tests.

Table 1. Scaling laws used for this study

Parameter	Unit	Scale factor (model/prototype)
Acceleration	m/s²	50
Velocity (dynamic)	m/s	1
Displacement	m	1/50
Stress	Pa	1
Strain	1	1
Force	N	$1/50^2$
Moment	N·m	$1/50^3$
Bending stiffness	N·m²	$1/50^4$
Axial stiffness	N	$1/50^2$
Time (dynamic)	s	1/50
Time (quasi-static)	s	$1/50^2$
Frequency	Hz	50

2.1 Soil mass

The physical model was constructed inside a laminar shear beam (LSB) container with internal dimensions of 720 × 380 mm and a reference height of 340 mm. The LSB consists of twenty-six superposed aluminium frames separated by cylindrical bearings designed to minimize shear resistance between layers, thereby reducing the influence of the container on the soil column's shearing behaviour (Esmaeilpour et al., 2023). In the following, the process for the model preparation is described.

2.1.1 Base Layer

The base layer was composed of dense Hostun sand (HN31) with a thickness of 80 mm, serving as a stiff bearing stratum into which the rigid inclusions (RI's) were embedded to achieve end-bearing tip conditions. The sand was prepared by air pluviation and had a relative density of 80%. The sand was subsequently saturated under vacuum pressure with de-aired water. Table 2 summarizes the physical properties of the sand. The purpose of using water for saturation is the accelerated pore pressure dissipation which minimizes the risk of liquefaction.

Table 2. Physical properties of the base layer Hostun sand layer.

Symbol	Description	Value
D_r	Relative density	80%
γ_d	Dry unit weight	15.09 kN/m³
e_0	Initial void ratio	0.69

2.1.2 Clay Layer

A 180 mm-thick soft clay layer was placed above the sand base. It consisted of three 60 mm sublayers prepared from a mixture of 80% Speswhite Kaolin and 20% Fontainebleau sand (NE34). The mixture was first prepared as a slurry (water content of 60%), which was poured into the container until a thickness of 85 mm. It was then preconsolidated at 1g under a vertical stress reaching 120 kPa, selected to achieve an undrained shear strength of 20 kPa and the required thickness of 60 mm. This formulation was adopted following earlier experimental work by Baudouin, (2010), and Khemakhem, (2012). The physical properties of the clay before and after consolidation are summarized in Table 3.

Table 3. Physical properties of the clay layer before and after 1g consolidation.

Condition	Water content w (%)	Void ratio e_0	Density ρ (kg/m³)
Before consolidation	60	1.584	1603
After consolidation	34	0.97	1776

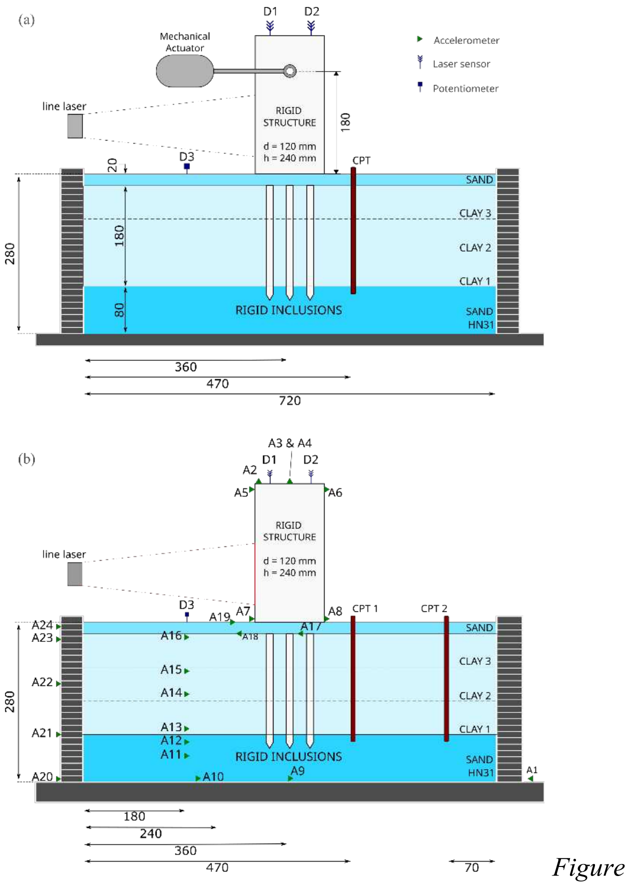

Figure

Figure 1. Layout of the (a) quasi-static and (b) dynamic centrifuge tests.

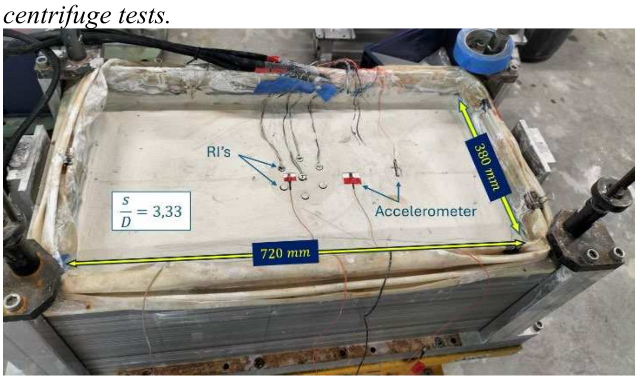

Figure 2. Photo of the disposition of the RI's (plan view)

2.1.3 Load Transfer Platform

The load transfer platform (LTP) ad a thickness of 20 mm and was constituted of a well-graded sand mixture of four Hostun sand fractions (HN38, HN34, HN31, and HN 0.4-0.63). The material was prepared with a water content of 5% and compacted using a falling hammer followed by trimming to ensure a smooth, level surface. Table 4 summarizes the physical properties of the LTP after compaction.

Table 4. Physical properties of the LTP sand.

Symbol	Description	Value
ρ	Moist density	1600 kg/m³
w	Water content	5%
D_r	Relative density	80%

2.2 Rigid inclusions

After full consolidation of the clay, seven aluminium RI's were installed under 1g conditions, directly after removing consolidation pressure, using a guide and a jack. This allowed precise vertical insertion at a constant rate of 0.1 mm/s, minimizing disturbance to the surrounding soil. Figure 3 illustrates the geometry of the inclusions. Each inclusion was 200 mm long with an external diameter of 12 mm, and a conical tip forming an angle of 60°, and a flexural and axial stiffnesses of 39 N.m^2 and 2.56 MN, respectively. The RI's were scaled to represent prototype reinforced concrete RI's of equivalent flexural and axial stiffnesses of 244 MN.m^2 and 6.39 GN. The RI's were installed at a spacing of 3.33D, greater than the recommended spacing of 3D to not consider group effects, and smaller than the maximum recommended value of 6D to ensure load transfer. Four of them were instrumented with strain gauges to measure internal bending moments and axial forces (Figure 3).

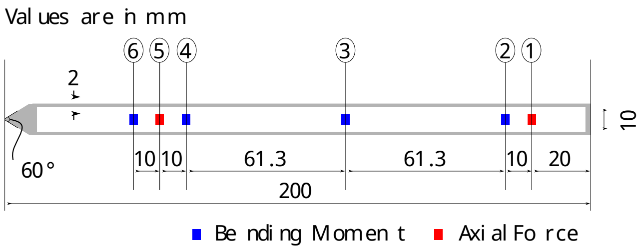

Figure 3. Cross-section view of the RI's used at model scale

2.3 Rigid structure

The superstructure was modelled as a rigid cylindrical mass designed to have a much higher fixed-base frequency than the natural frequency of the soil column obtained from free-field tests. The height of the centre of gravity was selected to ensure that rocking and rotational deformation would govern the response. Table 5 summarizes the main properties of the building at model and prototype scales.

The bearing capacity of a shallow foundation with a diameter similar to the existing structure, supported by the same RI system, was evaluated following ASIRI (2012). It reaches 130.4 kPa (SF = 3.25), compared to 90.3 kPa (SF = 2.25) without RIs.

Table 5. Physical properties of the rigid structure considered

Symbol	Description	Model	Prototype
H_0	Total height	24 cm	12 m
H_{cg}	Height of centre of gravity	18 cm	9 m
D	Base diameter	12 cm	6 m
m	Mass	1.318 kg	164.8 tonnes
f_0	Resonant frequency	400 Hz	8 Hz

2.4 Quasi-static pushover test

A quasi-static pushover test was performed on the slender structure placed on a RI reinforced ground. Figure 5 illustrates the apparatus for the quasi-static pushover test. The loads were applied using a mechanical actuator that was fixed on two support beams. A displacement controled horizontal loading was applied at the height of the gravity center of the building, using a "fork" shaped component connected to a force measuring sensor. The applied lateral load and displacement time histories are shown in Figure 4. Two and a half loading cycles with increasing displacement amplitude were imposed.

The loading amplitude was chosen based on the failure criterion proposed by Alcala-Ochoa et al., (2024) for a ground reinforced by RI's supporting a footing of similar diameter as the present structure. It was chosen such that the M-H couple applied on the foundation goes beyond the failure criterion (264.7 kN, 2382.5 kN.m) to mobilize the soil's resistance and observe the response of the system under ULS conditions. The loading rate is sufficiently low to assume quasi-static conditions and a drained response of the clay.

To monitor the response, two vertical point lasers were installed above the structure for rotations and settlements. Two cameras were fixed as well, one facing the structure and one fixed diagonally on one of the support beams. Unfortunately, the latter collapsed during the spin-up of the centrifuge. A potentiometer was placed at the ground level to observe the differential settlements between the structure and the soil.

2.5 Dynamic tests

In the dynamic tests, the container was instrumented by accelerometers, inside the soil, as well as on the structure, to monitor the dynamic response of the structure. The container was placed inside a servo-hydro-mechanical shaking table (Chazelas et al., 2008) and was injected by a sequence of twenty ground motions. A more-in-detail presentation of the dynamic test is given in Nohra et al., (2024a,b).

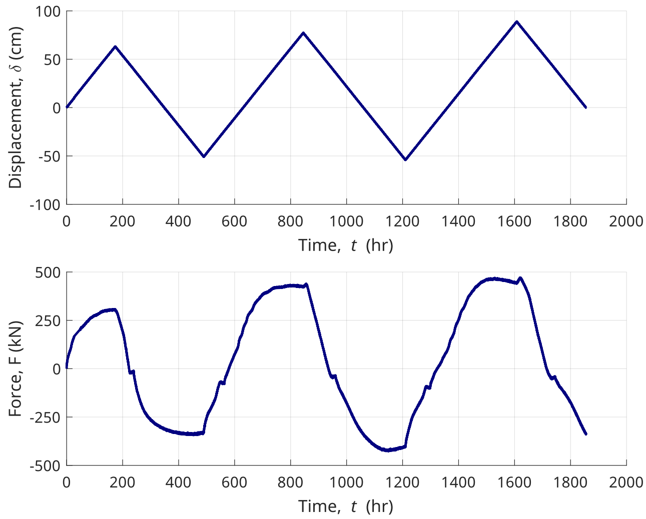

Figure 4. Time history of the horizontal displacement and force applied during the quasi-static pushover test.

3 RESULTS FROM CENTRIFUGE TESTS

It is important to note that loading was applied after 2 hrs of in-flight consolidation, that aimed to ensure the maximum effective stress and stiffness in the clay. All results are presented at prototype scale unless otherwise stated.

3.1 Quasi-static pushover test

3.1.1 Response of the Structure

Figure 6 shows the moment-rotation and the settlement-rotation relationship at the base of the structure. Settlements are computed as the average of the two lasers Overturning moments were determined as the sum of moments due to the horizontal force applied by the actuator on the structure, with that from the weight of the structure and the horizontal displacement (P-δ). The M-θ curves are highly nonlinear, showing a stiff response at very small rotation angles. Non-linearity starts to appear early as the rotation angle increases showing that the elastic response is limited only to very small values of θ. As rotation angles increase, the rotational stiffness starts to decrease s. The curves also indicate that the loading-unloading response shape shows a hysteretic behaviour, which shows that the system dissipates thanks to hysteresis damping, which can be evaluated through the area of each loop.

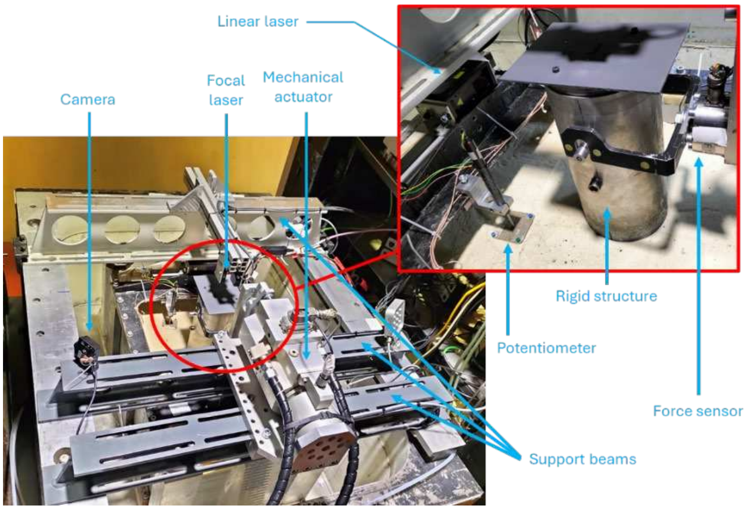

Figure 5. Quasi-static pushover test apparatus in the centrifuge.

The ultimate moment (M_{ult}), defined as the plateau value reached in the M - θ response during each displacement-controlled loading phase, increased progressively over successive loading cycles. This value represents the moment capacity of the system under monotonic loading. M_{ult} reached 3.67 MN·m after the first half-cycle. The value obtained is larger than that estimated from the failure criterion of Alcala-Ochoa et al., (2024), in **Erreur ! Source du renvoi introuvable.** thanks to the P-δ (additional overturning moments caused by the weight and the large rotations of the structure) effects that were considered to determine the values of ultimate moment. This shows that using the failure criterion provides conservative design limits.

The value of M_{ult} increased to 5.02 MN·m and then 5.5 MN·m (i.e., increases of 37% and 50%) after the second and third cycles. This increase can be attributed to the "capacity overstrength" observed during cyclic loading (Gajan and Kutter, 2008; Panagiotidou et al., 2012). It results from the combined effect of soil-foundation interaction mechanisms mobilized during large rotations and the contribution of P-δ effects. During loading, failure mechanisms develop beneath the footing, leading to soil rounding at the soil-foundation interface. Upon load reversal, the foundation must first surmount the hill formed from soil bulging. In addition, while the P-δ effects undermine the resisting moment during loading, they can enhance it during unloading. Together, these mechanisms imply that a greater moment is required during unloading to achieve the same rotation angle as during loading, thereby explaining the observed overstrength. After each cycle, the rate of increase in M_{ult} becomes smaller.

Regarding settlements, the shape of the curves reveals a soil rounding effect (Kokkali et al., 2015), showing a slightly uplifting-dominated response observed from the w-θ "horn"-shaped form at large values of θ. It can also be seen that permanent settlements accumulate but at a decreasing rate with each cycle. In addition, the amount of settlement reduction associated with soil rounding increases and the uplifting response becomes stronger. This indicates the initiation of plasticity and irreversible deformations in the system, which could stabilize after few cycles.

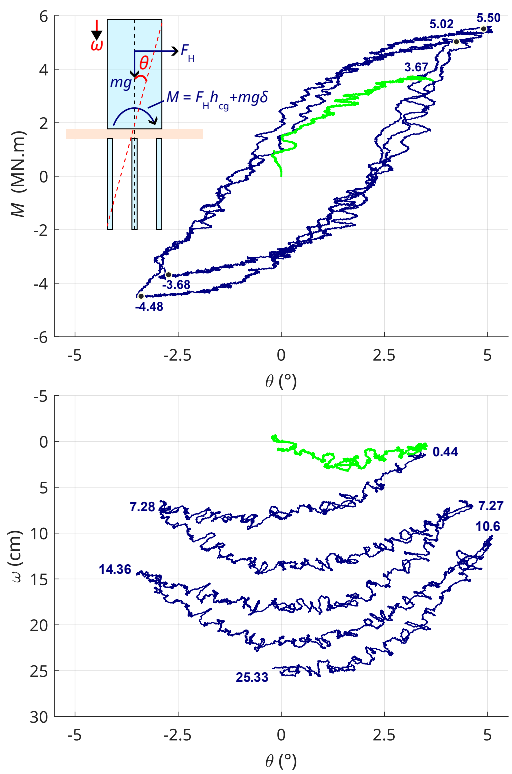

Figure 6. M–θ and ω–θ curves obtained from the quasi-static pushover test.

3.1.2 Internal Forces in the RI's

Figure 7 shows the results obtained in terms of bending moments at different locations inside the RI. The bending moments in the central RI's (RI's 1 and 4) are almost perfectly superposed, displaying a clear 'S' shape. This indicates that upon reaching a rotation threshold (≈3°), similar angle to that observed in Figure 7 at which stiffness decreases. Therefore, this can be explained by the strong non-linearities and reduction in soil-foundation rotational stiffness that limit additional soil arching and load transfer to occur. no additional bending moments are transferred to the central RI's.

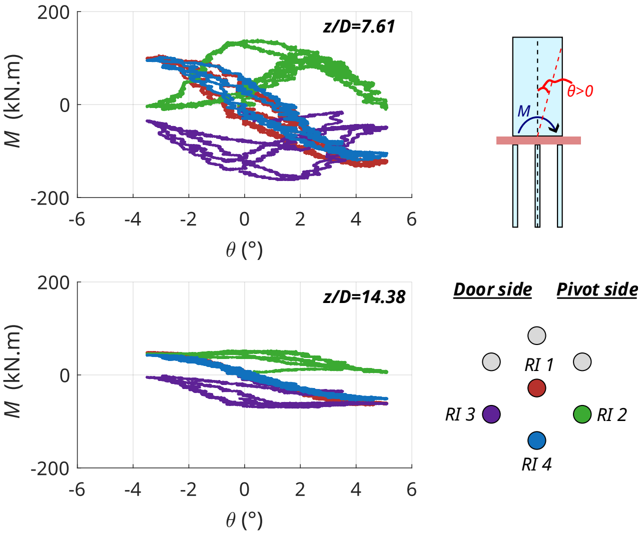

Figure 7. Evolution of bending moments in the RI's during the quasi-static pushover test.

In terms of axial forces (Figure 8), the central RI's exhibit a symmetrical 'butterfly shape' response. During increasing structural rotations, axial forces rise to a peak before uplift of the structure reduces load transfer on the central RI's while increasing it on the lateral RI in the direction of rotation. The axial forces transmitted to RI2 remains consistently higher than those in RI3 after each loading cycle. This asymmetry is attributed to the initial half-cycle of rotation toward RI2, which influenced subsequent force transmission. After the second and third cycles, axial stresses in RI2 were approximately 50% greater than in RI3. When a certain rotation angle is reached towards one of the lateral RIs, the axial force in the opposite RI stabilises. This indicates a complete loss of load transfer due to uplift and the presence of residual axial forces on the RI on which load transfer is not occurring. This behavior is likely attributable to residual friction. The residual axial forces measured in RI-2 and RI-3 were 48.8 kN and 24.6 kN at $z/D = 1.67$, and 63.4 kN and 81.9 kN at $z/D = 13.55$, respectively, indicating the development of permanent negative skin friction, which may be explained by the consolidation of the clay layer around the RI's.

3.2 Dynamic test

Figure 9 illustrates the evolution of the peak overturning moment per loading cycle as a function of the peak dynamic rotation ($\theta_{\max}$) during all ground motions: earthquakes (Figure 9a) and sinusoidal (Figure 9b) excitations. Moments were determined using the acceleration response computed at the centre of gravity of the structure through the equation:

$$M = m\ddot{a}h_{\text{cg}} \tag{1}$$

Dynamic rotations were computed using displacements obtained after filtering and integrating twice the accelerations. Also illustrated is the monotonic curve obtained from the quasi-static pushover test. It corresponds to the response during the first half-cycle of loading ($t < 200$ hr).

At very small rotation angles, the data points initially follow the slope corresponding to the maximum rotational stiffness ($K_{\text{r,max}}$). As the rotation angle increases and nonlinear effects develop, the secant stiffness ($K_{\text{r,sec}}$) decreases. Under both earthquake and low-amplitude sinusoidal excitations (0.05 g), the response slightly moves away from the monotonic curve but follows in the same trend, even at larger rotation amplitudes, particularly evident for the 1 Hz, 0.05 g sine case. By contrast, the response lies below the monotonic curve for excitations at 1 Hz – 0.15 g and 1 Hz – 0.25 g, exhibiting a significantly lower $K_{\text{r,sec}}$. This reduction can be attributed to soil softening, which may be due to nonlinear mechanisms, such as the accumulation of permanent residual rotations. This leads to a reduction in the mobilized ultimate moment, M_{ult}, under dynamic loading, which explains the deviation from the monotonic curve.

Peak dynamic overturning moments reach about 1226 kN·m, corresponding to approximately 33% of the peak moment obtained from quasi-static pushover tests conducted under monotonic soil conditions (not considering the reduced dynamic ultimate moment).

4 CONCLUSIONS

In this paper, quasi-static and dynamic centrifuge tests were conducted to evaluate the non-linear rocking response of a slender and rigid structure placed on a RI reinforced soft clay ground. The quasi-static pushover test was conducted such that the moment-force couple applied on the foundation exceeded the failure criterion of the foundation system considered and the dynamic test aimed at uncovering the effect of amplitude and frequency of the ground motion on the rocking response of the structure on RI's. The main conclusions are as follows:

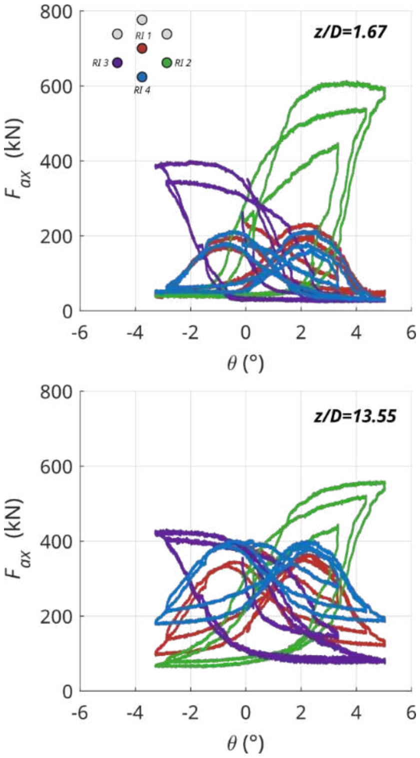

Figure 8. Evolution of axial forces in the RI's vs rotation angle.

- The response of the system is non-linear, as during quasi-static pushover and dynamic tests, the rotational stiffness decreases as the rotational angle increases.

Concerning the cyclic test:

- A capacity overstrength was observed after the first cycle where a higher moment is required to reach the same rotation angle, which could be caused by soil rounding and a modification of the P-δ effects.
- The response during cyclic loading starts slightly uplifting dominated with a reduction in the rate of settlement and a change to greater uplifting after each cycle.
- The initial rotation toward RI2 leads to axial forces about 50% higher in RI2 than in RI3, and beyond a critical rotation the opposite RI loses load transfer due to uplift.

Concerning the dynamic test:

- The response in terms of M-θ follows the monotonic pushover curve across most earthquake and sinusoidal excitations, except for the 1 Hz excitations at 0.15g and 0.25g, where a reduction in the effective ultimate moment was observed due to non-linearity.
- Under dynamic loading, the mobilized maximum moment reaches about 1226 kN.m, that correspond to 33% of the undegraded quasi-static pushover ultimate moment, excluding the degradation effects observed under 1 Hz sinusoidal excitation.

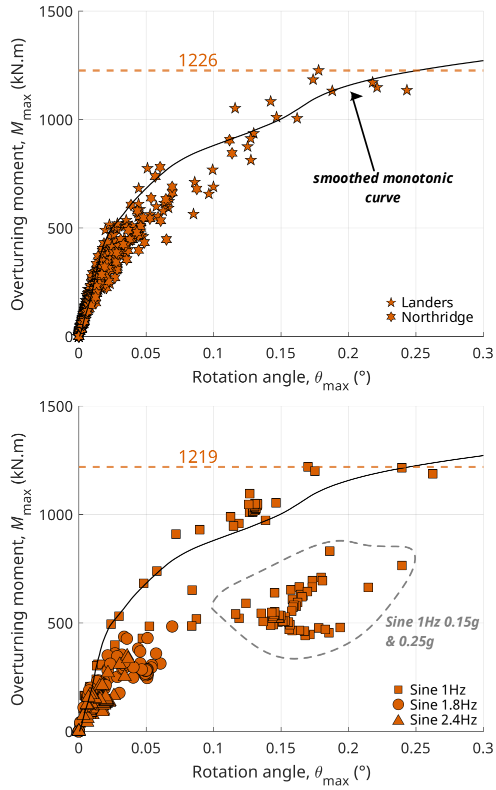

Figure 9. Evolution of peak overturning moment with peak dynamic rotation angle during all ground motions of the series: (a) earthquakes and (b) sines.

ACKNOWLEDGEMENTS

The authors want to thank the French National Research Agency for funding the ASIRIplus_SDS project (ANR-19-C22-0015), as well as the Pays de la Loire region and the Gustave Eiffel University for the Ph.D grant. Special thanks to the GERS-CG technical team as well.

REFERENCES

Alcala-Ochoa, R., Li, Z., Kotronis, P., & Sciarra, G. (2024). 3D failure envelope of rigid inclusion reinforced foundations. *Acta Geotechnica*, 1–20. https://doi.org/10.1007/s11440-024-02309-9

ASIRI, (2012). *Recommendations for the Design, Construction and Control of Rigid Inclusion Ground Improvements*. Presses des Ponts et Chaussées.

Baudouin, G. (2010). *Sols renforcés par inclusions rigides : Modélisation physique en centrifugeuse de remblais et de dallage* [Doctoral dissertation, École doctorale Sciences pour l'ingénieur, Géosciences, Architecture, Nantes,FRANCE]. http://www.theses.fr/2010NANT2046

Briançon, L. (2004). *Etat des connaissances: Amélioration des sols par inclusions rigides. ASEPGI 2004, PaRI's*.

Chazelas, J., Escoffier, S., Garnier, J., Thorel, L., & Rault, G. (2008). Original technologies for proven performances for the new lcpc earthquake simulator. *Bulletin of Earthquake Engineering*, 6, 723–728. https://doi.org/10.1007/s10518-008-9096-z

Esmaeilpour, P., Mamazizi, A., & Madabhushi, G. S. (2023). An overview of the model container types in physical modeling of geotechnical problems. *Soil Dynamics and Earthquake Engineering*, 168, 107827. https://doi.org/10.1016/j.soildyn.2023.107827

Gajan, S., & Kutter, B. L. (2008). Capacity, settlement, and energy dissipation of shallow footings subjected to rocking. *Journal of Geotechnical and Geoenvironmental Engineering*, 134(8), 1129–1141. https://doi.org/10.1061/(ASCE)1090-0241(2008)134:8(1129)

Garnier, J., Gaudin, C., Springman, S. M., Culligan, P. J., Goodings, D., Konig, D., ... & Thorel, L. (2007). Catalogue of scaling laws and similitude questions in geotechnical centrifuge modelling. *International Journal of Physical Modelling in Geotechnics*, 7(3), 01-23. https://doi.org/10.1680/ijpmg.2007.070301

Ha, J.-G., Ko, K.-W., Jo, S.-B., Park, H.-J., & Kim, D.-S. (2019). Investigation of seismic performances of unconnected pile foundations using dynamic centrifuge tests. *Bulletin of Earthquake Engineering*, 17, 2433–2458. https://doi.org/10.1007/s10518-018-00530-y

Khemakhem, M. (2012). *Etude expérimentale de la réponse aux charges latérales monotones et cycliques d'un pieu foré dans l'argile* [Doctoral project]. Ecole Centrale de Nantes. https://theses.fr/2012ECDN0026

Kokkali, P., Abdoun, T., & Anastasopoulos, I. (2015). Centrifuge modeling of rocking foundations on improved soil. *Journal of Geotechnical and Geoenvironmental Engineering*, 141(10), 04015041. https://doi.org/10.1061/(ASCE)GT.1943-5606.0001315

Liang, F., Li, T., Qian, Y., Wang, C., & Jia, Y. (2021). Investigating the seismic isolation effect of the cushioned pile raft foundation in soft clay through dynamic centrifuge tests. *Soil Dynamics and Earthquake Engineering*, 142, 106554. https://doi.org/10.1016/j.soildyn.2020.106554

Loli, M., Knappett, J., Brown, M., Anastasopoulos, I., & Gazetas, G. (2015). Centrifuge testing of a bridge pier on a rocking isolated foundation supported on unconnected piles. *6th International Conference on Earthquake Geotechnical Engineering*, 362.

Nohra, C., Sorino-Camelo, C., Escoffier, S., Li, Z., & Thorel, L. (2024a). Experimental study of the kinematic interaction between a cohesive soil and a group of rigid inclusions through dynamic centrifuge tests. *Japanese Geotechnical Society Special Publication*, *10*(25), 936-941. https://doi.org/10.3208/jgssp.v10.OS-14-05

Nohra, C., Soriano-Camelo, C., Escoffier, S., Li, Z., & Thorel, L. (2024b). Dynamic centrifuge modelling of the effect of a superstructure on the dynamic response of rigid inclusions. In *5th European Conference on Physical Modelling in Geotechnics*. https://doi.org/10.53243/ECPMG2024-15

Panagiotidou, A. I., Gazetas, G., & Gerolymos, N. (2012). Pushover and seismic response of foundations on stiff clay: Analysis with P-delta effects. *Earthquake Spectra*, *28*(4), 1589-1618. https://doi.org/10.1193/1.4000084

Pecker, A. (2004). *Design and construction of the rion antirion bridge*. In Geotechnical engineering for transportation projects (pp. 216–240). https://doi.org/10.1061/40744(154)7

Pecker, A. (2006). Enhanced seismic design of shallow foundations: Example of the rion antirion bridge. *4th Athenian lecture on Geotechnical Engineering*, 1. https://www.gefyra.gr/images/user/Publications/4th%20Athenian%20Lecture.pdf

Pecker, A. (2023b). Interrelationships between practice, standardisation and innovation in geotechnical earthquake engineering. *Bulletin of Earthquake Engineering*, 21(6), 3091–3132. https://doi.org/10.1007/s10518-023-01669-z

Satheeshkumar, T., Sanjit, B., Prasun, H., & Sourabh, R. (2025). A comprehensive review on the dynamic behaviour of connected and nonconnected pile-raft foundations. *Journal of Earthquake Engineering*, 29(4), 865–900. https://doi.org/10.1080/13632469.2024.2446507

Yang, Y., Fan, H., Cheng, Y. P., Gong, W., Dai, G., Liang, F., & Jia, Y. (2022). Seismic response of nuclear power station with disconnected pile-raft foundation using dynamic centrifuge tests. *Journal of Cleaner Production*, 379,134572. https://doi.org/10.1016/j.jclepro.2022.134572

Yang, Y., Cheng, Y. P., Gong, W., Fan, H., & Dai, G. (2023). Effect of cushion types on the seismic response of structure with disconnected pile raft foundation. *Structures*, 48, 1333–1345. https://doi.org/10.1016/j.istruc.2022.12.099